

Supplementary information

Adaptation of the PTI equation for a focused laser beam with Gaussian beam profile

Here, we calculate the phase shift in our modulated single-beam PTI (MSPTI) for a fundamental (or TEM₀₀) transverse Gaussian mode. This calculation can be expanded to other beam profiles, if the profile is known. Figure S1 shows the intensity profile along the direction of propagation z for a focused beam with a TEM₀₀ mode profile. The focal point of the beam is arbitrarily set to $z = 0$, which we assume to be located in the centre of the measurement chamber of length $2a$.

The intensity I (units of W m⁻²) in the chamber is given by

$$I(r, z) = I_0 \left(\frac{w_0}{w(z)} \right)^2 e^{-\frac{2r^2}{w(z)^2}} \quad (\text{S1})$$

where r is the radial distance from the central axis of the beam and z is the propagation axis with the focal point at $z = 0$. $w_0 = w(z = 0)$ is the waist of the laser beam in the focal point, and $w(z)$ is given by

$$w(z) = w_0 \sqrt{1 + \left(\frac{z}{z_r} \right)^2}, \quad (\text{S2})$$

and depends on the Rayleigh distance

$$z_r = \frac{\pi w_0^2}{\lambda} \quad (\text{S3})$$

The total laser power (units of W) is

$$P = \frac{I_0}{2} (w_0)^2 \pi \quad (\text{S4})$$

In analogy to the calculation presented in Sedlacek (2006), the induced phase change is calculated in an infinitesimally small toroidal volume $dV = 2\pi r \cdot dr \cdot dz$. For an absorption coefficient b_{abs} the absorbed power within dV is

$$dP_{abs} = I(r, z) \cdot b_{abs} \cdot 2\pi r \cdot dr \cdot dz \quad (\text{S5})$$

During the heating time Δt , the induced temperature change within dV is

$$\Delta T = \frac{dP_{abs}}{dm c_p} \Delta t = \frac{I(r, z) \cdot b_{abs}}{\rho \cdot c_p} \Delta t \quad (\text{S6})$$

where dm , c_p and ρ are the infinitesimal mass, heat capacity and density of the air, respectively. The induced phase change from dV is

$$d\Delta\varphi = \frac{2\pi dz}{\lambda} \Delta n = \frac{2\pi dz}{\lambda} (n - 1) \frac{\Delta T}{T} = \frac{2\pi}{\lambda} (n - 1) \frac{I(r, z) \cdot b_{abs}}{T \cdot \rho \cdot c_p} \Delta t \cdot dz \quad (\text{S7})$$

For calculating the total phase change $\Delta\varphi$, one needs to account for the z dependence of the intensity in the chamber and weigh $d\Delta\varphi$ with a weighting factor before integrating over the entire volume. This weighting factor is the normalized intensity $\frac{I(r, z) 2r\pi}{\frac{I_0}{2} (w_0)^2 \pi}$ with $\iint \frac{I(r, z) 2r\pi}{\frac{I_0}{2} (w_0)^2 \pi} dr dz = 1$.

The integration over the measurement chamber volume yields

$$\Delta\varphi = \int_{-a}^{+a} \int_0^\infty \frac{I(r, z) 2r\pi}{\frac{I_0}{2} (w_0)^2 \pi} \cdot I(r, z) \frac{2\pi}{\lambda} (n - 1) \frac{b_{abs}}{T \rho c_p} \Delta t \cdot dr \cdot dz \quad (\text{S8})$$

30 Combining S8 with S1-S4 and using the identities $\int_0^\infty r e^{-\frac{4r^2}{w(z)^2}} dr = \frac{w(z)^2}{8}$ and $\int_{-a}^{+a} \frac{z_r^2}{(z^2+z_r^2)} dz = 2z_r \arctan\left(\frac{a}{z_r}\right)$
 one finally finds

$$\Delta\varphi = \frac{2\pi \cdot (n-1)}{\lambda \cdot T \cdot \rho \cdot c_p} \cdot \frac{2P_0}{\lambda} \cdot \arctan\left(\frac{a}{z_r}\right) \cdot b_{abs} \cdot \Delta t \quad (\text{S9})$$

In the following paragraph we present an example calculation for a 10 cm long ($a = 5$ cm) sample chamber. Figure S1a shows for a constant laser power of $P = 100$ mW the illuminance in the beam centre ($r = 0$) as a function of the chamber
 35 length position z , where the laser beam is focused in the centre of the chamber ($z = 0$), for a number of different beam waists w_0 .

For a heating time of $\Delta t = 5.5$ ms (91 Hz modulation), and absorption coefficient $b_{abs} = 10^{-4}$ m⁻¹ and air at standard conditions, Figure S1b presents the corresponding spatial contribution to the measured phase shift, i.e. $\frac{d\Delta\varphi}{dz} = \frac{2\pi(n-1)}{\lambda \cdot T \cdot \rho \cdot c_p} \cdot$

$\frac{I_0}{2} \frac{z_r^2}{(z^2+z_r^2)} \cdot b_{abs} \cdot \Delta t$, within this chamber. An integration over the chamber (from $z = -5$ cm to $z = 5$ cm) yields
 40 sensitivities of $\frac{2P}{\lambda} \cdot \arctan\left(\frac{a}{z_r}\right) = 586, 573, 520$ and 347 kW m⁻¹ for $w_0 = 0.01, 0.02, 0.04$ and 0.08 mm, respectively.

This example illustrates that focussing at the correct position is important to centre and focus the sensitive region into a well-confined range and to lower signal background contributions from the chamber windows.

Description of signal processing methodology

The rate of change of phase during the heating cycle is determined by two processes. Firstly, the linear heating process
 45 arising from the absorption of light within the beam volume and secondly, by the exponential cooling of the beam volume driven by the temperature difference to the surroundings. The effect of these two competing processes is that the beam volume reaches an equilibrium temperature. The rate of the phase change for the PTI developed in this work is found to be empirically best approximated with an exponential function of the form:

$$\Delta\varphi(t_{heat}) = a \left(1 - e^{-\frac{t}{\tau}}\right) + c \quad (\text{S10})$$

50 where the parameter a is the limit of the phase change and is defined as the phase shift at which the heating rate due to absorption and cooling rate due to heat loss out of the beam volume are equal, τ is the mean lifetime of the cooling process and c is the offset from phase quadrature. The parameter τ is characteristic for the system and is dependent on the pump beam focusing and the pump/probe beam geometry, and the thermal diffusivity of the sample gas (Monson et al., 1989).

55 An example of a 1-second average of experimental data for a soot concentration of approximately 100 $\mu\text{g m}^{-3}$ is shown in Figure S2. The experimental data has been offset corrected by firstly subtracting c and then $\Delta\varphi$ measured in a pure argon atmosphere to remove the PTI contributions from the interferometer optics, leaving just the absorption dynamics of the sample.

The heating curves were analysed for a range of different concentrations of electrical discharge generated BC and the
 60 results of the fits are shown in Figure S3. By comparing the a and τ values from the fits for a range of concentrations it was found that τ remained constant within experimental error, and that a showed a linear relationship with soot concentration. This can also be understood directly from the definitions of these values: τ is dependent on the laser

beam geometry and thus the time required for heat from light absorption to leave the beam volume. The beam geometry did not change between measurements and so τ is observed to remain virtually constant. The parameter a is directly related to the heat increase of the beam volume due to light absorption and is therefore expected to vary linearly with the absorption coefficient, i.e. the concentration of the absorbing species.

At $t \sim 0$ the heat losses out of the beam volume are negligible and a near linear increase of $\Delta\varphi$ is observed with time.

The rate of increase of $\Delta\varphi$ for $t \sim 0$ is given by

$$\frac{\Delta\varphi}{\Delta t} = \frac{a}{\tau} \quad (\text{S11})$$

In Figure S4, the exponential fit from Figure S2 is plotted together with fitted a and a line of the form:

$$\Delta\varphi(t_{heat}) = \frac{a}{\tau}t + c \quad (\text{S12})$$

The best linear fits to the heating curves were also determined. A comparison of the results obtained from the exponential and linear fits to the heating curves in terms of $\frac{d\Delta\varphi}{\Delta t}$ is shown in Figure S5. The results of the exponential fits are presented as $\frac{a}{\tau}$ as per Equation S12. Both sets of fits show a clear linear relationship with eBC concentration, with the rate of increase of the exponential fits a factor of approximately 2.7 higher than that of the linear fits. As $\frac{d\Delta\varphi}{\Delta t}$ is calibrated to b_{abs} via a gas of known absorption (NO_2 in this case), the absolute value of the fitted rate of increase is unimportant, so long as the value determined for $\frac{d\Delta\varphi}{\Delta t}$ increases linearly with b_{abs} . This linear relationship has been demonstrated for both the exponential and linear fitting methods, thus validating the use of the linear fitting methodology.

80 **Physical layout of the single-beam photothermal interferometer**

See Figure S6 for a photographic representation of the MSPTI.

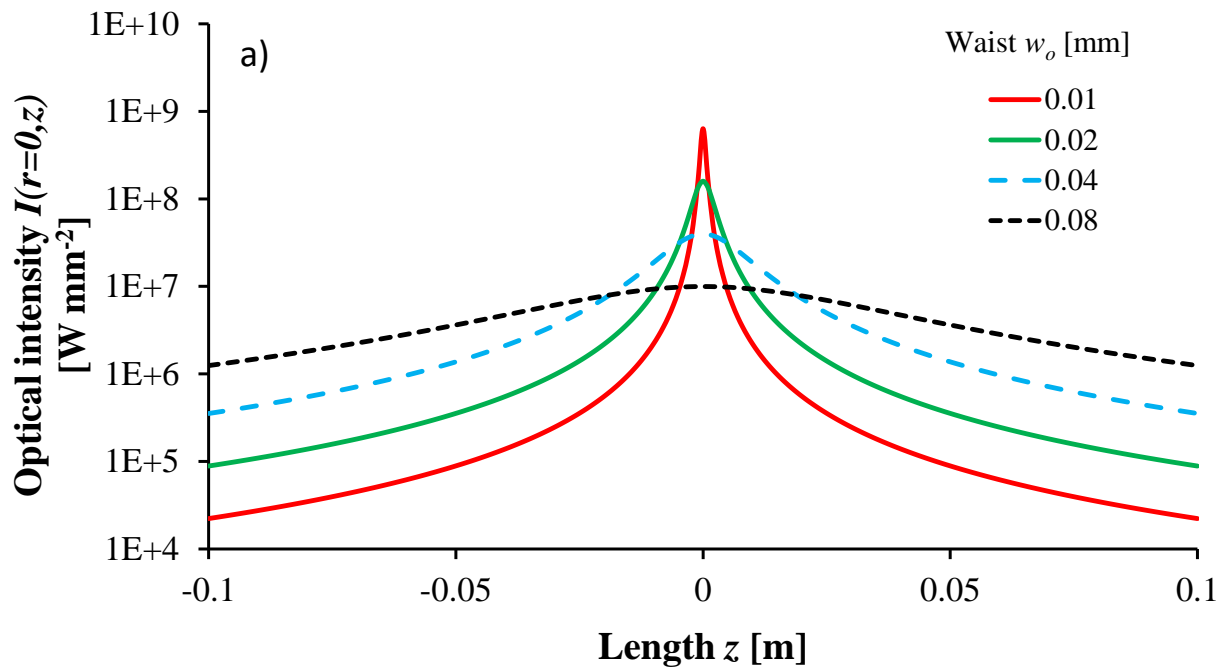
Raw data for calculation of standard deviation and drift

See Figure S7 for the best least-squares linear fit to the raw data for the subtraction of the linear drift.

References

85 Monson, B., Vyas, R., and Gupta, R.: Pulsed and cw photothermal phase shift spectroscopy in a fluid medium: theory, Appl. Opt., 28, 2554-2561, 10.1364/AO.28.002554, 1989.

Sedlacek, A. J.: Real-time detection of ambient aerosols using photothermal interferometry: Folded Jamin interferometer, Rev. Sci. Instrum., 77, 10.1063/1.2205623, 2006.



90

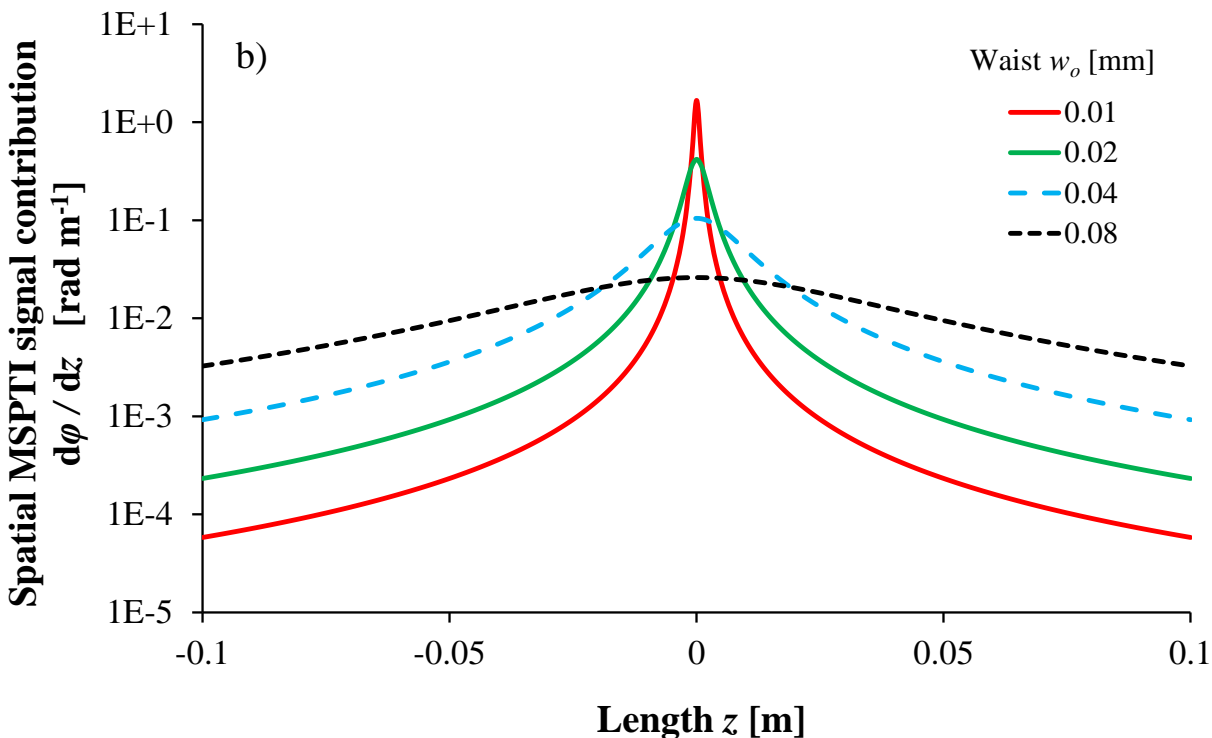


Figure S1: The optical intensity of the laser beam along the propagation axis z is shown in a). The position of the focus has been set to $z = 0$. In b) the spatial contribution to the MSPTI signal is plotted as a function of z . The localisation of the signal contribution around the focal point as the beam waist decreases shows the importance of the positioning of the sample chamber. Note the log scale on the y-axis.

95

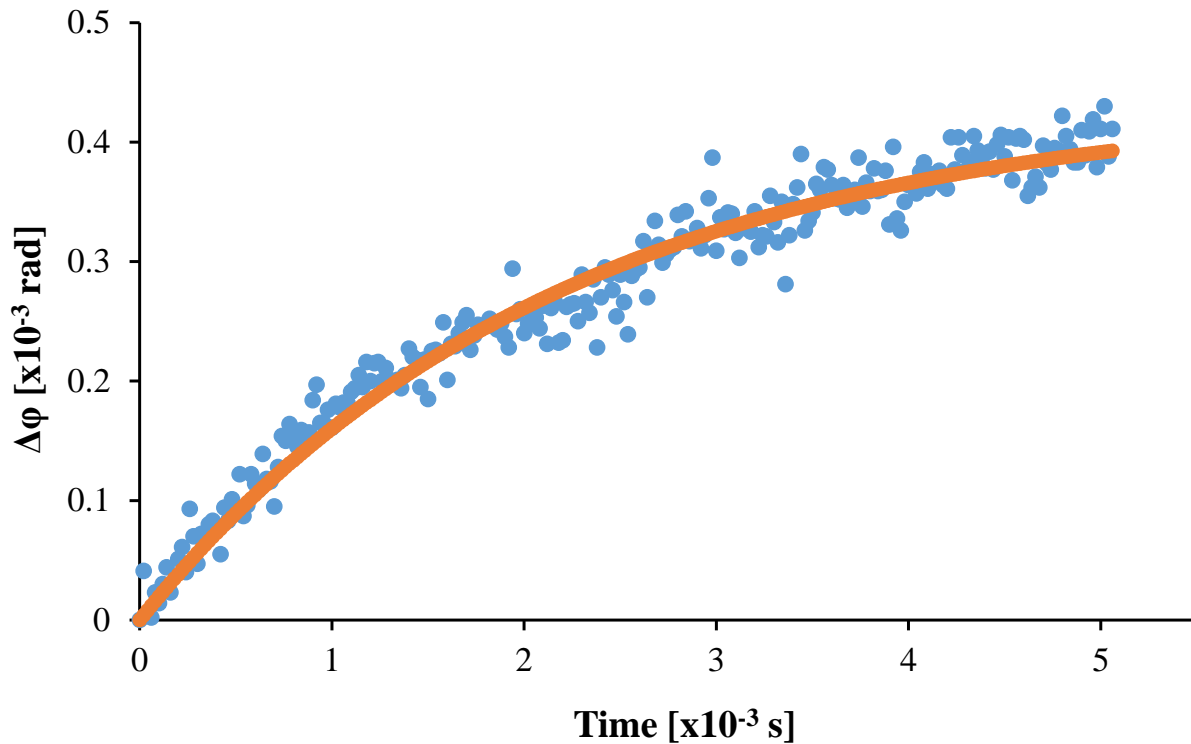
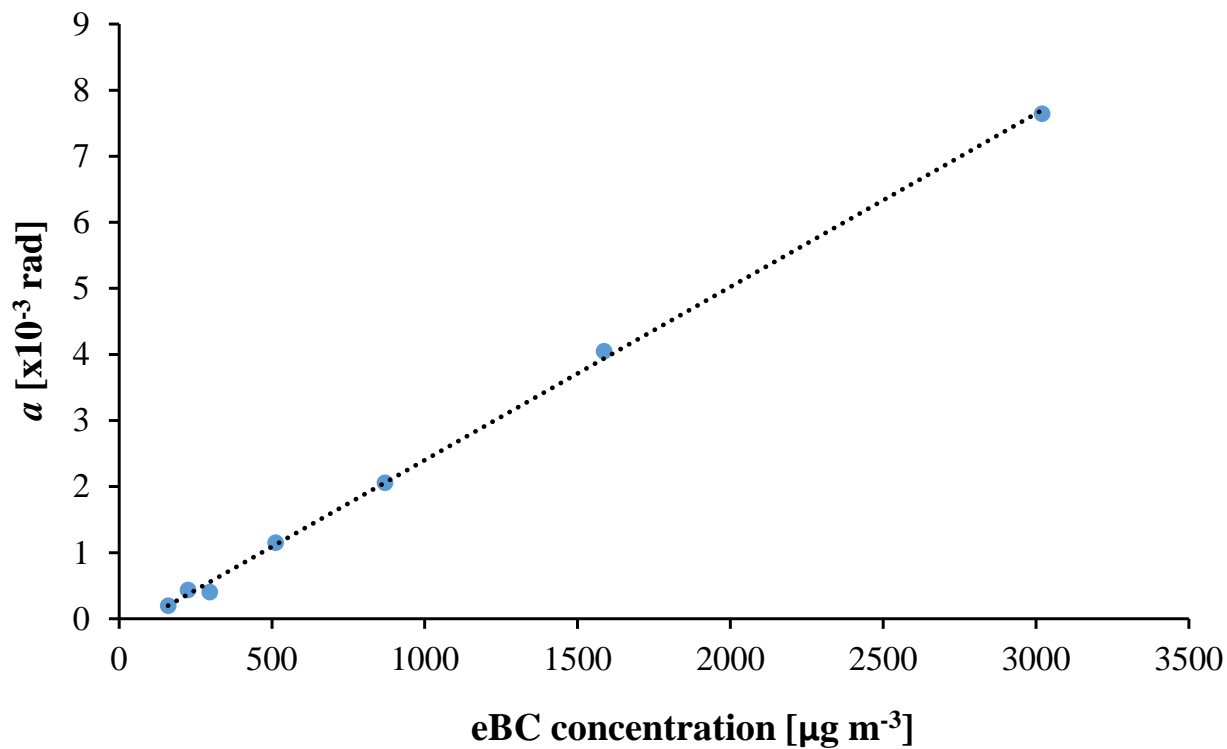
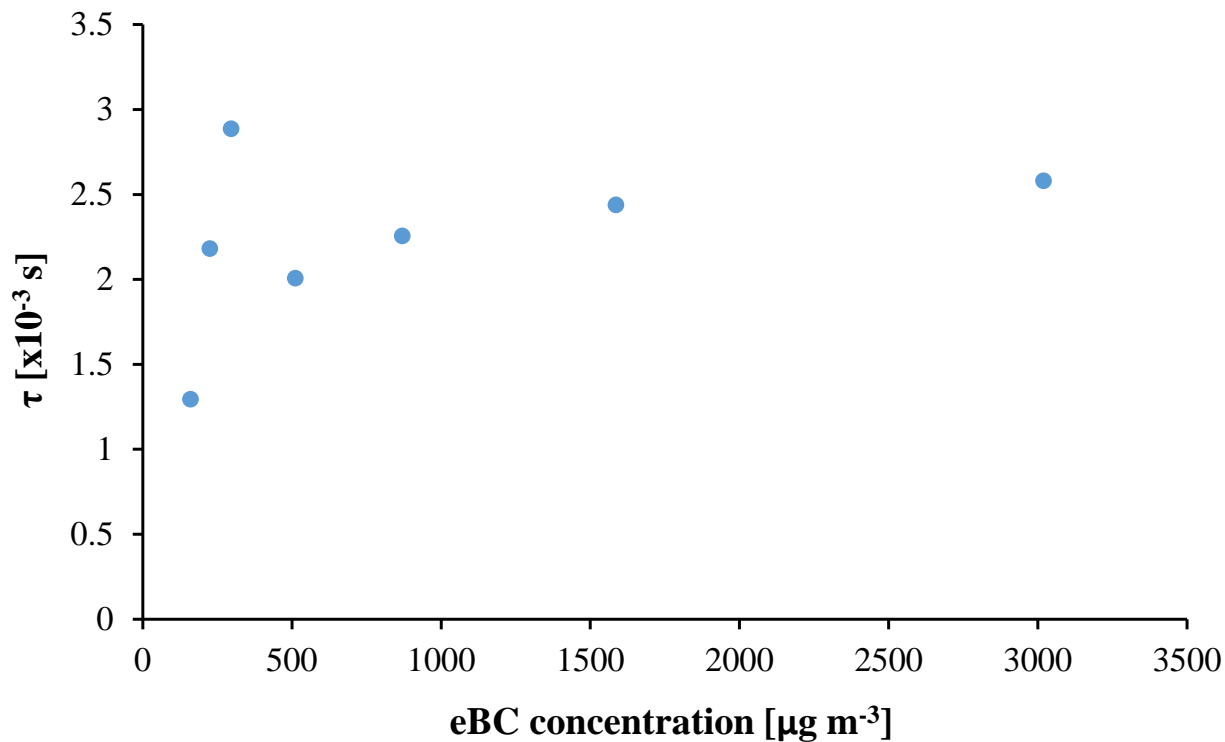


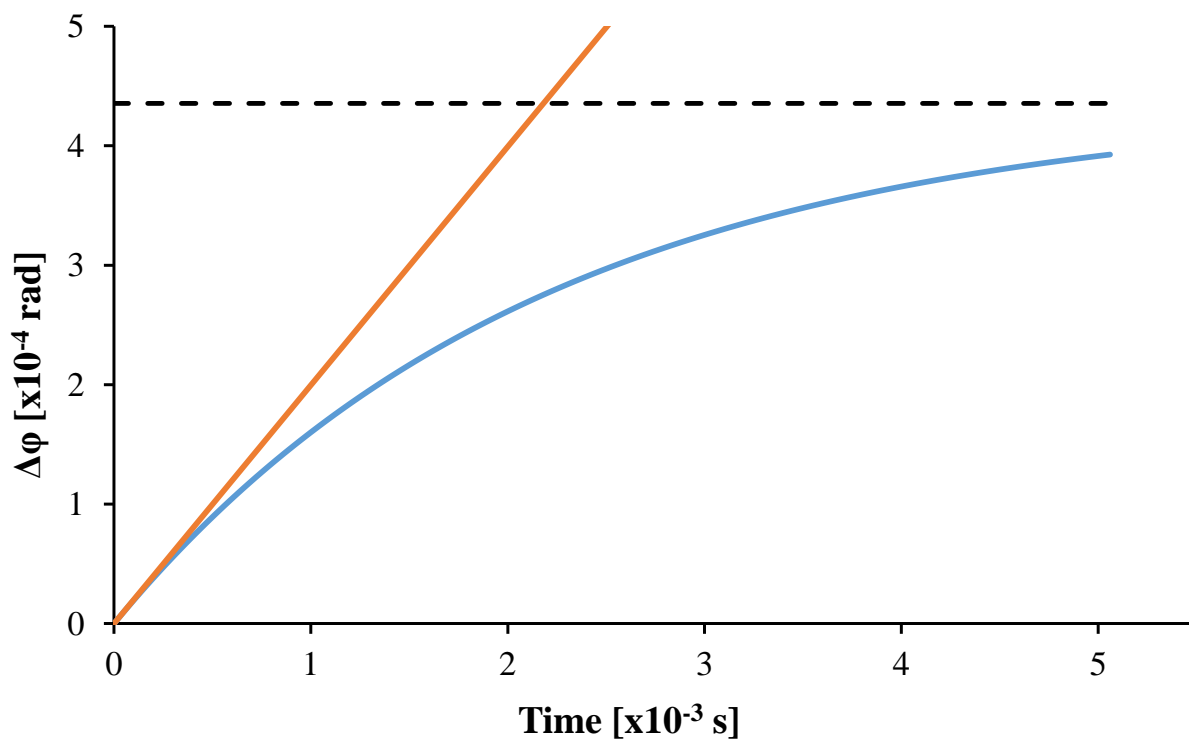
Figure S2 – 1-second average of a typical heating cycle for a soot concentration of approximately 100 $\mu\text{g m}^{-3}$. The red line represents the best exponential fit to the data.

100





105 Figure S3 – Variation of the parameters a and τ with eBC concentration. eBC concentration was measured using an AE33. The data points represent a fit to the heating curves averaged over 1 second and the dotted line in a) is the best least-squares linear fit to the data.



110 Figure S4 – Exponential fit from Figure S2 (blue) plotted together with fitted a (black dashed) and a line of the form of Equation S2.3 (red) using fitted a and τ . Notice the good fit of the fitted exponential curve and line below $t = 0.5$ ms.

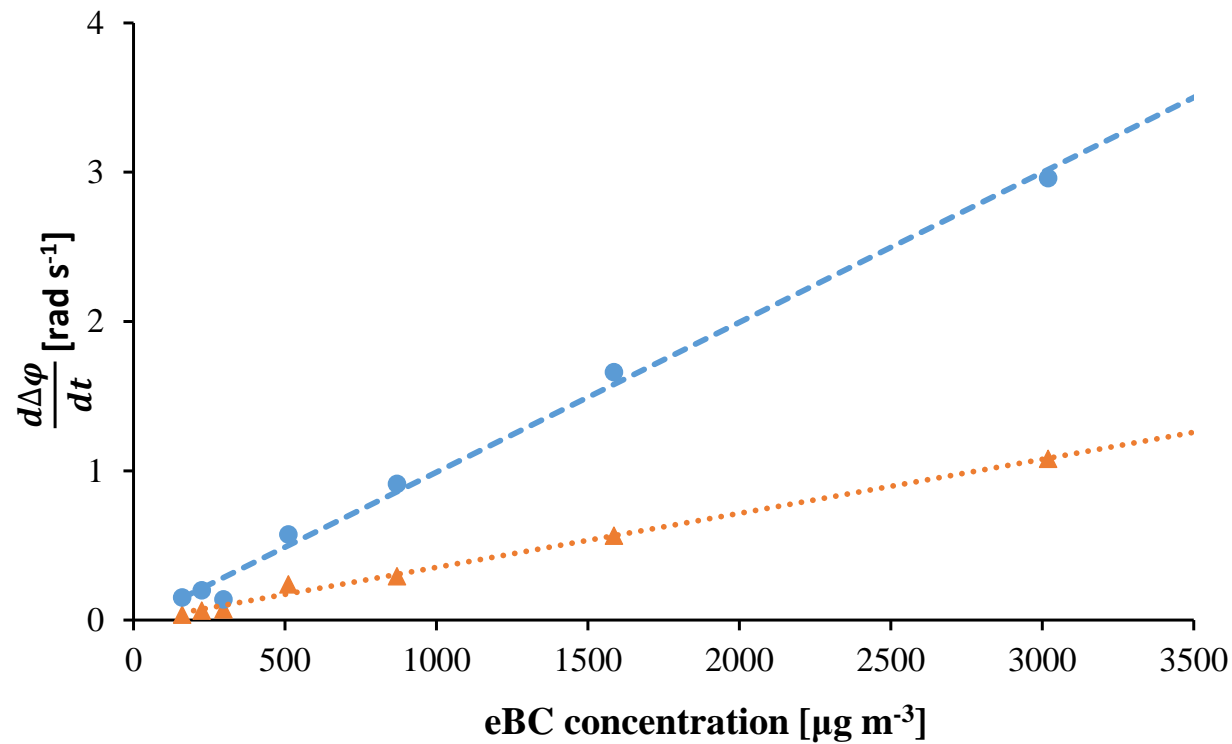


Figure S5 – Evaluated values of $\frac{d\Delta\phi}{dt}$ for a range of eBC concentrations using the exponential (blue circles) and linear (red triangles) fitting methodologies. The lines represent the best least squares fit to the respective data sets. See the accompanying text for further details.

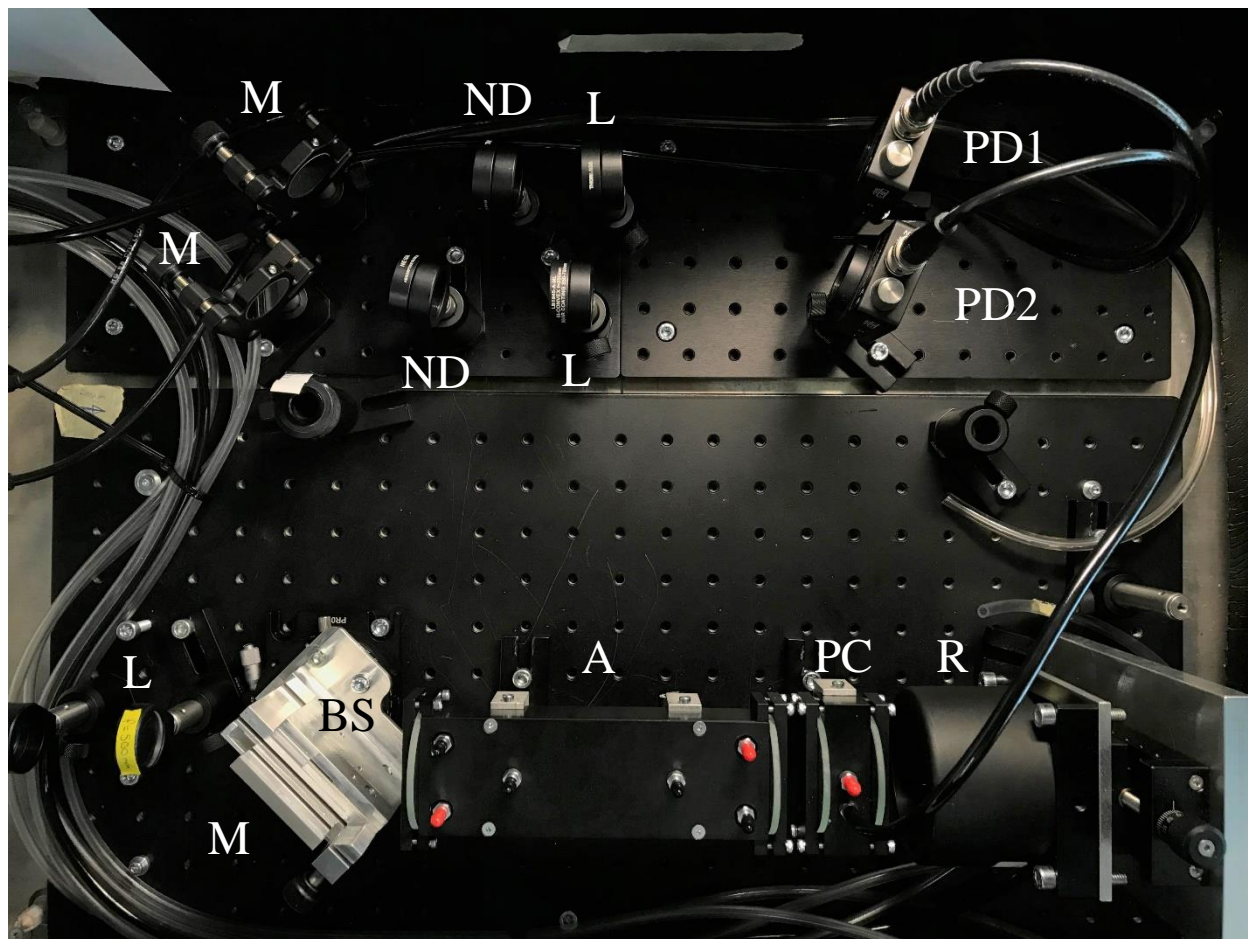


Figure S6 – A photograph showing the construction of the experimental apparatus. The components are labelled as followed: L is a single-element lens, M a mirror, BS a beam splitter, AC the aerosol chamber, PC the pressure chamber, RR a retroreflector, ND a neutral density filter and PD1 and PD2 are photodiode detectors. The tubing for the aerosol chamber has been left disconnected for clarity.

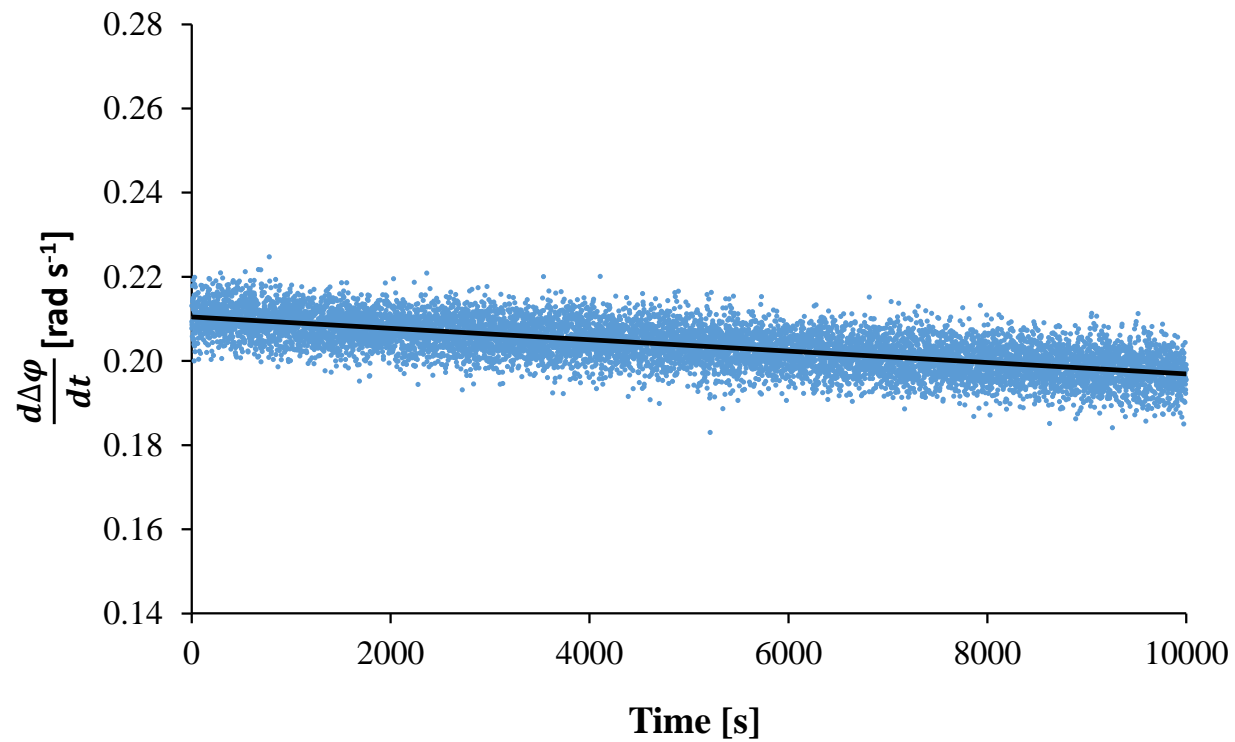


Figure S7 – Raw data for the determination of the baseline drift. The data points are 1 second averages and the black line is the best linear fit to the data. The drift was subtracted from the raw data before calculation of the detection limits for the instrument.